Title

Mechanical Competence and Bone Quality Develop During Skeletal Growth

Journal

Journal of Bone and Mineral Research, 34(8)

ISSN

0884-0431

Authors

Zimmermann, Elizabeth A

Riedel, Christoph

Schmidt, Felix N

et al.

Publication Date

2019-08-01

DOI

10.1002/jbmr.3730

Peer reviewed

Mechanical competence and bone quality develop during skeletal growth

Authors: E. A. Zimmermann[1], C. Riedel[1], F. N. Schmidt[1], K. E. Stockhausen[1], Y. Chushkin[2], E. Schaible[3], B. Gludovatz[4], E. Vettorazzi[5], F. Zontone[2], K. Püschel[6], M. Amling[1], R. O. Ritchie[4,7], B. Busse[1]*

Affiliations:

[1]Department of Osteology and Biomechanics, University Medical Center, Hamburg, Germany.

[2]Beamline ID 10, European Synchrotron Radiation Facility, Grenoble, France.

[3]Experimental Systems Group, Advanced Light Source, Berkeley, CA, USA.

[4]Materials Sciences Division, Lawrence Berkeley National Laboratory, Berkeley, CA, USA.

[5]Department of Medical Biometry and Epidemiology, University Medical Center, Hamburg, Germany.

[6]Department of Forensic Medicine, University Medical Center, Hamburg, Germany.

[7]Department of Materials Science and Engineering, University of California, Berkeley, CA, USA.

Word count: 3,951

Number of pages: 29

Number of figures: 5

***To whom correspondence should be addressed:**

Björn Busse, Ph.D.

Department of Osteology and Biomechanics

University Medical Center Hamburg-Eppendorf
Lottestr. 55a
22529 Hamburg, Germany
E-mail: b.busse@uke.uni-hamburg.de.

Disclosures: The authors have no competing financial interests with the research presented in this study.

Abstract

Bone fracture risk is influenced by bone quality, which encompasses bone's composition as well as its multi-scale organization and architecture. Aging and disease deteriorate bone quality leading to reduced mechanical properties and higher fracture incidence. Largely unexplored is how bone quality and mechanical competence progress during longitudinal bone growth. Human femoral cortical bone was acquired from fetal (n=1), infantile (n=3), and 2-14 year-old cases (n=4) at the mid-diaphysis. Bone quality was assessed in terms of bone structure, osteocyte characteristics, mineralization, and collagen orientation. The mechanical properties were investigated by measuring tensile deformation at multiple length-scales via synchrotron x-ray diffraction. We find dramatic differences in mechanical resistance with age. Specifically cortical bone in 2-14 year-old cases exhibits a 160% greater stiffness and 83% higher strength than fetal/infantile cases. The higher mechanical resistance of the 2-14 year-old cases is associated with advantageous bone quality, specifically higher bone volume fraction, better micron-scale organization (woven *vs.* lamellar) and higher mean mineralization compared to fetal/infantile cases. Our study reveals that bone quality is superior after remodeling/modeling processes convert the primary woven bone structure to lamellar bone. In this female cohort, the microstructural differences at the femoral diaphysis were apparent between the 1-2 year-old cases. Indeed, the lamellar bone in 2-14 year-old cases had a superior structural organization (collagen and osteocyte characteristics) and composition for resisting deformation and fracture than fetal/infantile bone.

Mechanistically, the changes in bone quality during longitudinal bone growth lead to higher fracture resistance because collagen fibrils are better aligned to resist tensile forces, while elevated mean mineralization reinforces the collagen scaffold. Thus, our results reveal inherent weaknesses of the fetal/infantile skeleton signifying its' inferior bone quality. These results have implications for pediatric fracture risk, as bone produced at ossification centers during longitudinal bone growth could display similarly weak points.

Keywords: Bone modeling, bone remodeling, osteocytes, bone quality, analysis/quantitation of bone, histomorphometry

Introduction

Bone's resistance to fracture is highly dependent on its bone quality, which encompasses the bone volume fraction, microstructural organization, damage, and nano-scale composition.[1] Indeed, aging and disease (such as osteoporosis, osteogenesis imperfecta, Paget's disease of bone, osteomalacia due to vitamin D deficiency, *etc.*) are linked to genetic, environmental and disease-related factors that alter bone quality and in turn affect fracture resistance.[2–9] In terms of aging, high fracture incidence is found not only in elderly individuals, but also in children and adolescents during longitudinal skeletal growth (<20 years).[10] 30% of children experience at least one bone fracture, with roughly two-thirds of fractures occurring from low-energy traumas.[11–15] In contrast to elderly individuals where fracture risk increases due to imbalances in bone resorption and formation, increased fracture risk in children/adolescents has been postulated to be the result of a transitory weakness in the skeleton.[16,17] However, bone quality and mechanical competence at the tissue level during skeletal growth remain largely unexplored.

Like other materials, bones resist fracture through their multi-scale structure that imparts resistance to deformation and crack growth. At the nanoscale, collagen and mineral assemble into fibrils, which promote strength and plastic deformation through

mechanisms such as fibrillar stretching/sliding, sacrificial bonding and nano-/micron-scale cracking.[7,18–20] At the scale of hundreds of microns, secondary osteons resist crack propagation in mature tissue through crack deflection and crack bridging mechanisms.[21,22] Aging- and disease-related changes in bone quality, such as the mineralization or cross-linking profile at small length-scales or the osteon density at larger length-scales, have been shown to reduce the effectiveness of these mechanisms that resist deformation and fracture in bone.[6–9]

While the main mechanisms of fracture resistance in mature bone tissue have been identified, it is unclear if the same mechanisms are active in longitudinally growing bone due to potential differences in bone quality. Most bones, particularly the long bones, vertebrae and ilium, grow in length through *endochondral ossification*. Endochondral ossification progresses at ossification centers (*e.g.,* growth plates), where the extracellular matrix (ECM) surrounding the hypertrophic chondrocytes calcifies followed by chondrocyte apoptosis. Then, the remaining calcified ECM is used as a scaffold for the formation of bone, termed primary spongiosa or primary bone.[23–25] Later during the growth process and throughout life, the tissue structure is refined through *bone remodeling*, where cylindrical units of tissue 200-300 μm in diameter are resorbed by bone cells and filled-in with new highly organized bone tissue called *secondary osteons*. However, the exact timing of bone remodeling in the primary spongiosa is not known.[25,26] While endochondral ossification increases bone length, changes in bone diameter and cortex thickness occur during growth and throughout life through *bone modeling* processes by apposition or resorption at the periosteal and endocortical surfaces.[27,28]

Here, we investigate how bone quality and mechanical competence

develop during skeletal growth. The chosen skeletal site is the femoral mid-diaphysis because the same region can be investigated at different stages of maturity in different age groups.[29] Based on bone's present microstructural features during growth, the cases were split into two groups: i) fetal/infantile bone consisting of primary bone with no osteons and ii) 2-14 y.o. cases consisting of remodeled tissue (i.e., secondary osteons). Here, we investigate whether these two age groups associated with specific microstructural characteristics have critical differences in bone mechanical performance and quality. We hypothesize that the 2-14 year-old cases composed of osteonal bone will reveal a

greater mean mineralization and a more longitudinally aligned collagen fibril network providing superior mechanical resistance in comparison to fetal/infantile cases composed of woven bone.

Methods

Materials: Cortical bone from the femoral mid-diaphysis was acquired from human cases. Individuals with bone pathologies that would affect bone quality or skeletal growth were not included in the study. This study has a cross-sectional design with bone samples originating from a Caucasian female cohort with the following ages: 22-weeks-of-gestation, n=1; 2 months, n=2; 1 year, n=1; 2 years, n=1; 5 years, n=1, 14 years, n=2). The study was conducted in accordance with the local ethics regulations[30] and approval by the State of Hamburg's General Medical Council Ethics Committee (WF-013/2011).

Histology: Femoral cross-sections were fixed in 3.7% formaldehyde for 3 days, dehydrated and embedded undecalcified in glycol-methacrylate (Technovit, Heraeus Kulzer GmbH, Wehrheim, Germany). Histological sections were removed with a rotation microtome (microTec, Techno-Med GmbH) and stained with von Kossa/van Gieson. Histomorphometry on stained sections was used to measure OV/BV (osteoid volume / bone volume), OS/BS (osteoid surface /

bone surface) and O.Th (osteoid thickness) using OsteoMeasure (OsteoMetrics, Decatur, GA).[31,32]

Circularly polarized light microscopy: Circularly polarized light (CPL) microscopy was used to assess the collagen fiber orientation.[33,34] Methylmethacrylate-embedded samples were ground to a thickness of 100 µm with an automatic grinding machine (Exakt, Norderstedt, Germany). Using an Olympus BX-61 microscope (Olympus, Hamburg, Germany) equipped with CPL filter sets, both brightfield and CPL images of the same ROI were captured in 8-bit grayscale.

A masking procedure was applied to separate bone and non-bone areas (e.g., porous spaces,

lacunae), which were assigned a gray value of 0.[33] The grayscale of the bone pixels in each masked CPL image was measured and reported as the average brightness (based on gray levels 1-255).[35] When viewing bone under polarized light, collagen fibers that run parallel to the plane of the section appear bright, while fibers that run perpendicular to it appear dark. Oblique collagen fibers result in intermediate grayscale values.[33,36]

Mineralization: The bone mineral density distribution (BMDD) was determined with quantitative backscattered electron imaging (qBEI).[37] The scanning electron microscope (LEO 435 VP, Leo Electron Microscopy Ltd., Cambridge, UK) was operated in backscattered mode at 20 kV and 680 pA with a constant working distance of 20 mm. A block containing the entire medial side of the cross-section was analyzed for each individual. Multiple images were taken at 50x magnification with a pixel size of 2.3 μm² and stitched prior to the histogram analysis. The gray level was calibrated with aluminum and carbon standards, such that the gray level was linearly proportional to calcium content (light and dark pixels correspond with high and low calcium content, respectively). The bone mineralization distribution was characterized by the mean, peak and standard deviation of the gray value distribution, which correspond to

the mean calcium content (Ca Mean, Wt-%), the peak calcium content (Ca Peak, Wt-%) and degree of variance/heterogeneity (Ca Width, Wt-%), respectively. From qBEI, the percentage of bone mineralized below the 5th percentile (Ca Low, % B.Ar.) or above the 95th percentile (Ca High, % B.Ar.) of a control BMDD, obtained from healthy individuals aged 31.4 ± 9.5 years, were calculated. Backscattered electron images were also used to calculate the cortical mineralized bone volume per tissue volume (BV/TV), the mean osteocyte lacunar area (Ot.Lc.Ar, µm²) and the number of osteocyte lacunae per bone area (N.Ot.Lc./B.Ar., #/mm²).

The mineral phase was also characterized with Fourier transform infrared (FTIR) imaging.

Histological sections of cortical bone with a 5-μm thickness were scanned in transmission with a

Spotlight 400 FTIR Imaging system (Perkin Elmer, Waltham, MA). One section of the entire

medial side of the cross-section was analyzed per individual. Spectra were acquired over a spectral

range of 570-4000 cm^{-1} at a 4-cm^{-1} spectral resolution with 32 scans/pixel. Images were scanned

at a 25-μm step size. The spectra were automatically corrected for atmospheric effects and noise

reduction. After background and PMMA subtraction, the FTIR parameters were calculated for

each spectrum. Specifically, the mineral-to-matrix ratio was calculated through the area ratio of

the amide I (1590-1725 cm^{-1}) and phosphate peaks (915-1180 cm^{-1}), the carbonate-to-phosphate

ratio through the area ratio of the carbonate (850-900 cm^{-1}) and phosphate peaks, as well as the

mineral maturity index through the area ratio of the 1030 cm^{-1} and 1110 cm^{-1} subbands.[38,39] For

each parameter at the individual level, the distribution of values was fitted with a Gaussian curve.

The mean value is reported for each FTIR parameter as well as the heterogeneity, which was

measured by the FWHM of the Gaussian curve.

Mechanical properties: Deformation at the tissue, fibril and mineral length-scales was

investigated with mechanical tensile tests during small and wide-angle x-ray scattering/diffraction

(SAXS/WAXD) experiments (**Fig. S1**) at beamline 7.3.3 at the Advanced Light Source

synchrotron radiation facility (Lawrence Berkeley National Laboratory, Berkeley, CA).[7,40,41]

Here, multiple mechanical tests were performed for each case (fetal n=2, 2 months n=2, 2 months

n=4, 1 year n=3, 2 years n=4, 5 years n=2, 14 years n =4), except one 14-year-old case due to a

lack of remaining material. Mechanical tests were performed on tissue from the posterior side of

the diaphyseal femur.

Tensile tests are performed to measure overall bone strength. Simultaneously, fibril and mineral strains are measured through x-ray scattering because bone's ordered nano-level structure (*i.e.,* fibril's 67-nm periodicity and mineral's crystal structure) diffracts x-rays allowing nano-scale deformation to be measured during tensile testing.[7,41] The experimental methods/analysis have been previously described.[7] Briefly, hydrated cortical tensile samples (15mm x 1mm x 250μm) were loaded in tension (TST350 tensile stage, Linkam Scientific Instruments, Surrey, UK) with SAXS/WAXD data collected for 0.3s every 10s during the tests. Pilatus detectors were positioned ~4000 mm from the sample to collect SAXS data and 150 mm from the sample with an 18-degree angle to collect WAXD data using a 10-keV x-ray energy.

The analysis software IGOR Pro (Wavemetrics, Portland, OR) and the custom macro NIKA were used to calibrate the image and convert 2D data to 1D.[42] Then, the first-order collagen peak and the mineral 002 peak in the 1D SAXS and WAXD datasets, respectively, were fit to detect changes in the average collagen and mineral d-spacing. The load was recorded during tensile testing and tissue stress was calculated by normalizing the load by the cross-sectional area.

Additionally, tissue strain was measured by imaging the change in spacing of horizontal lines

marked on the sample's surface, which were later analyzed using a custom-programmed image analysis software utilizing the software package Vision Assistant 8.5 (National Instruments, Austin, TX). For each individual, ≥2 samples were tested with SAXS/WAXD. For each sample, the tissue stress, mineral strain and fibril strain data were binned every 0.1% tissue strain and averaged on the individual level. The average and standard deviation are reported.

Synchrotron coherent diffraction x-ray imaging (CDI): CDI was performed at beamline ID10 at the European Synchrotron Radiation Facility (Grenoble, France) on a 2-month-old and 14-year-old case. CDI results in a 3D image of the bone fragment. Methyl-methacrylate was removed

from histological sections with 2-methoxyethyl acetate followed by an alcohol series and demineralized water. Then, fragments of the bone sections were deposited onto Si $_3N_4$ membranes (Silson, Northampton, UK). The samples were rotated between tilts of -75° and 75° at 0.5° step sizes and the 2D diffraction pattern was taken at each step with 8-keV coherent x-rays. The 2D diffraction patterns were combined into a 3D diffraction pattern. A phase retrieval algorithm was applied to reconstruct the 3D electron density distribution from the 3D Fourier intensity data with a 14.7-nm voxel size.[43] The 2D image stack was filtered and thresholded to isolate large extrafibrillar mineralization. Then, the volume of each mineral particle was measured with FIJI image analysis software.

Statistics: All data are represented as mean ± standard deviation (SD). Data were aggregated on the individual level by averaging and separated into two groups based on microstructural observations: the 2 - 14 year-old samples contained osteons and the fetal - 1 year-old samples did not. Due to the small sample size, a non-parametric statistical analysis was used. Data were aggregated on the individual level and the Mann-Whitney U test was carried out with a significance level of $\alpha = 0.05$ using SPSS Statistics.

Results

Bone quality during skeletal growth

Densification of the cortex In human cortical bone from the femoral mid-diaphysis, the bone volume fraction was analyzed with von Kossa/van Gieson-stained sections in a pediatric cohort.

In the fetal/infantile cases (**Fig. 1A,B**), the bone's micron-level structure resembles a scaffold with long porous channels and high amounts of unmineralized bone matrix (*i.e.,* osteoid). In contrast, the 2-14 year-old cases (**Fig. 1C,D**) exhibited a dense bone structure primarily consisting of

mineralized tissue, without extensive areas containing osteoid. The bone volume fraction in the 2-14 year-old cases was 22% higher than the fetal/infantile cases (p=0.03) (**Fig. 1E**). Additionally, bone formation decreased with age, with a 90% higher osteoid volume and 71% higher osteoid surface in the fetal/infantile bone *vs.* the 2-14 year-old cases (p=0.03) (**Fig. 1F,G**). However, the osteoid thicknesses were similar in both age groups, which suggests similar mineralization processes (**Fig. 1H**). A higher osteocyte lacunar density in the early phase of osteogenesis (*i.e.,* in woven bone) with shorter dendritic processes and no particular alignment within the bone matrix is evident (**Fig. 1I**), while the size of the osteocyte lacunae is larger in fetal – 1. y.o. cases in comparison to 2-14 y.o. cases (**Fig. 1J**). These histological data are also shown in **Fig. S5A-F** as a function of age, where the same trends can be seen between the fetal/infantile cases and the 2-14 year-old cases.

Organization of collagen fibers The porous bone scaffold in fetal/infantile cases and the dense bone structure in the 2-14 year-old cases were investigated in terms of collagen fiber organization with quantitative polarized light microscopy (**Figs. 1K-O, S2, S5G**). Here, collagen fibers that are transversely aligned appear bright and fibers that are longitudinally aligned appear dark. In fetal and infantile cortical bone, the scaffold-like microstructure has an

unorganized collagen fiber
39
40
structure, with packets of dark and bright collagen fibers (**Fig. 1L,M**). This
4
type of collagen fiber
42
43
organization reflects woven bone. While woven bone dominates the
fetal/infantile cases, the 2-14
44
45
year-old cases consisted of secondary remodeled osteonal bone (**Fig. 1N,O**).
Here, the remodeled
46
47
osteonal bone consists of secondary osteons with alternating bright and dark
4
lines, called lamellae.
49
50
These lamellae represent highly organized layers of collagen fibers. The
alternating brightness
51
52
signifies that the collagen fibers in neighboring lamellae alternate in
orientation. Quantitative
53
54
analysis of the brightness in the polarized light microscopy images (**Figs. 1K,**
S5G) shows that the

5
5
5
6
5
7

fetal/infantile cases have a significantly higher brightness indicating greater transversal collagen alignment than the 2-14 year-old cases. This implies that the collagen fibers are becoming preferentially longitudinally oriented in the 2-14 year-old cases.

Homogenization and elevation of mineral distribution Trends in the amount and distribution of mineral with age during skeletal growth were investigated with quantitative backscattered electron imaging (qBEI) (**Fig. 2**), where the calcium content scales with the gray value (high mineralization: bright, low mineralization: dark). Here, in the fetal/infantile cases (**Fig. 2A,B**), the calcified cartilage precursor formed during endochondral ossification is visible within the scaffold (white arrows), due to its higher mineral content than the newly formed bone. Comparatively, in 2-14 year-old cases, secondary osteons indicative of *bone remodeling* at the femoral mid-diaphysis are visible (**Fig. 2C,D**) with qBEI by their circular appearance, darker color (from lower mineralization), and highly mineralized outer boundary (*i.e.,* cement line). QBEI analysis of the gray value histograms (**Fig. 2E**) indicate that the Ca Mean mineralization increases with age, such that Ca Mean is 10% greater in the 2-14 year-old cases than the fetal/infantile cases (**Figs. 2F, S6A)**; however, no significant difference was found for Ca Peak (**Figs. 2G, S6B**). The high

mineralization of the fetal case can be attributed to the high level of calcified cartilage. Further analysis of the Ca Width, which assesses the heterogeneity in the bone mineral density distribution (**Figs. 2H, S6C**), indicated a decrease in the heterogeneity with age that was 34% lower in the 2-14-year-old cases. Furthermore, the primary bone has a greater proportion of low mineralized tissue under development than remodeled bone but each have similar proportions of high mineralized tissue (**Figs. 2I,J, S6D,E**).

These trends in mineralization are also visible in Fourier transform infrared (FTIR) spectroscopy images of the mineral-to-matrix ratio (MMR) (**Figs. 3, S3**). Here, the MMR increases

with age, such that it is 12% lower in the fetal/infantile cases (**Figs. 3E, S7A**). The heterogeneity of the MMR parameter also was significantly lower in the 2-14 year-old cases (**Fig. S7D**). These trends in the MMR follow the complementary measurements in the Ca Mean, reported above. The carbonate-to-phosphate ratio (CPR) and the mineral maturity were also computed from the FTIR spectrum (**Figs. 3F,G**; **S3C,D; S4; S7**) but neither showed a significant trend.

3D nanostructural images of the 2-month-old and 14-year-old samples were produced using synchrotron coherent diffraction imaging (CDI). Here, fibrils are visible with their characteristic 67-nm banding pattern (**Fig. 4A,B**). Additionally, large extrafibrillar mineral platelets are observed on the fibrils' surface (**Fig. 4C**). The extrafibrillar mineral accounted for 3.1% of the volume in the 2-month-old sample and 5.3% in the 14-year-old sample. The distribution of extrafibrillar mineral volumes followed a log-normal distribution (**Fig. 4D**). While all extrafibrillar mineral particles were generally plate-shaped with a 41-44-nm thickness, the 2-month-old cases contained smaller mineral crystals (largest cross-section: 0.19 x 0.10 μm^2) than the 14-year-old cases (largest cross-section: 0.45 x 0.36 μm^2).

Mechanical competence during skeletal growth

To investigate the multi-scale mechanisms governing bone deformation,

the mechanical resistance of the bone tissue from the pediatric cohort was measured at multiple length scales with tensile tests (measuring macro-scale deformation) during synchrotron small-angle x-ray scattering (SAXS) and wide-angle x-ray diffraction (WAXD) experiments (measuring deformation at the fibril and mineral levels, respectively) (**Fig. 5**). As load is applied in the tensile test, the tissue first behaves elastically with a linear relationship between stress and strain (**Fig. 5A,B**), which is characterized by the elastic modulus and mechanistically originates from stretching of molecular-

level bonds. Here, the modulus was 160% greater in the 2-14-year-old cases (**Figs. 5E, S8A**), in comparison with the fetal/infantile cases.

After elastic stretching, the material begins to non-linearly deform under mechanical load, which is characterized by permanent deformation (**Fig. 5A,B**). Here, the ultimate strength and failure strain describe the non-linear behavior. The ultimate bone strength again is 83% greater in the 2-14 year-old cases than the fetal/infantile cases (**Figs. 5F, S8B**). The failure strain trends toward lower values at higher ages; however, the differences were not significant (**Figs. 5G, S8C**).

The tissue's strength originates from deformation of its basic building blocks at the nanoscale. Here, mechanical loads applied to the tissue are transferred to the fibril, composed of collagen molecules and mineral nanoplatelets. Deformation in the fibril and mineral was measured during tensile tests with SAXS/WAXD. The fibril behavior was similar for each age group (**Fig. 5C**), where fibrils deform proportionally to applied tissue strain.

The differences in behavior at the nano-level are in the mineral deformation. WAXD measures tensile deformation in the mineral lattice of mineral platelets within and between collagen fibrils. As the samples are tested in tension, the mineral first stretches proportionally (i.e., linear relationship) to tissue strain (**Fig. 5D**). The slope of the linear portion of the

mineral vs. tissue strain curve increases with age, with a significantly greater value in the 2-14 year-old cases (**Figs. 5H, S8D**). Thus, the better micron-level organization (lamellar vs woven bone) in older cases may allow the mineral to deform more easily and contribute to the mechanical response. Then, in the fetal – 2 year-old samples, the linear relation between mineral and tissue strain becomes non-linear.

In the non-linear region, the mineral strain plateaus around 0.44% in the fetal – 1 year-old cases and at 0.6% in the 2 year-old case (**Fig. 5D**). At the plateau, the mineral strain is constant as the

tissue deforms, which may indicate sliding within/between fibrils or non-linear deformation in the collagen matrix.

Discussion

During childhood and adolescence, the growth and development of long bones involves longitudinal growth through endochondral ossification, changes in diameter through periosteal/endocortical apposition/resorption as well as bone remodeling. Our aim was to investigate bone quality and mechanical differences during the longitudinal growth of bones. Here, using the mid-femoral diaphysis at different ages during formation and maturation of the tissue, we investigated bone quality at a consistent skeletal site using high-resolution materials-science-based techniques and find that fetal/infantile bone tissue has an inferior bone quality and mechanical resistance than bone from 2-14 year-olds.

As the pediatric skeleton grows, the quality and form of the bone are shaped by ossification processes that grow the bone in length and in diameter as well as continue remodeling the existing structure. Fetal/infantile cases consisted of a porous, disorganized patchwork of collagen fiber orientations, characteristic of woven bone (**Fig. 1L,M**). Woven bone is known to be present during

longitudinal growth, bone fracture healing and bone modeling in adaptation to mechanical load.[25,44,45] The woven tissue consists of patches of collagen fibers with the same orientation, some oriented with the principal loading axis and others not (**Fig. 1L,M**). Conversely, highly organized lamellae found in secondary osteons were observed in the 2-14 year-old cases, which is a similar microstructural organization as adult bone. Indeed, studies in the development of long bones in mice show a similar porous scaffold-like cortex in fetal/infantile tissue with further densification near the time of walking.[46,47] Thus, investigation of the bone tissue at the femoral

mid-diaphysis reflects that endochondral ossification results in deposition of woven bone and that around the age of 1-2 years (**Fig. S5A,E**), bone remodeling processes replace the woven tissue with lamellar osteonal bone. This is also reflected by a similar collagen orientation in the age period of 2-14 years, possibly in response to changes in biomechanical loading.[34,36,48] Large differences in collagen orientation were observed in the fetal/infantile cases **(Fig. S5G)**. The fluctuation of the collagen orientation is linked to the disorganized nature of woven bone tissue and possibly due to the lower degree of mechanical stimuli experienced at this age.

The changes in bone quality during skeletal development additionally entail differences in the mineralization distribution. Specifically, the mean mineralization (Ca Mean) increased until about 2 years and then remained fairly constant with age (**Figs. 2, S6A).** As a result, the 2-14 year-old cases had a 10% greater Ca Mean and a 34% lower heterogeneity than the fetal/infantile cases.

Our data are in agreement with a recent study that found constant bone mineral density distribution in individuals between the ages of 1.5 to 23 years.[49] However, Currey et al.[50,51] found that ash content increased with age in children/adolescents. The bone mineral density distribution measured with qBEI may follow the same trends as the ash content.[52] Nevertheless, a discrepancy

may be present due to the low number of cases tested in the studies of Currey and coworkers.

While qBEI measures do not inform about the mineral characteristics on a large three-dimensional volume of bone tissue (as in ash content), the main benefit is that spatial compositional data is provided and thus, the distribution of mineral can be quantitatively assessed. The differences in the mineralization distribution between the fetal/infantile and 2-14 year-old cases may be related to the collagen fiber organization. In our study, the 2-14 year old cases consisted of secondary bone (*i.e.,* remodeled osteons); thus, it follows that the remodeling events may create a balanced mineral distribution as tissue is resorbed and renewed with age. Conversely, the fetal/infantile

cases consisted of patches of woven bone. This disorganized collagen fiber structure incorporates less mineral than lamellar bone and/or may have a shorter mineralization period due to its rapid deposition. Correspondingly lower mineralization has been measured in woven bone found in disease states, such as Paget's disease of bone and also in the bony callus formed during fracture healing.[8,44,53] CaLow exhibits similar trends with age as the collagen orientation (**Figs. S5G, S6E**). CaLow has a broad range of values in fetal/infantile bone, whereas in the 2-14 year range, CaLow is fairly constant. This may represent the influence of mechanical loading (e.g., walking) on the bone composition and structure.[54,55] After remodeling processes commence (2-14 year-old cases), which coincides with further biomechanical stimulation, the bone quality parameters (bone volume fraction, collagen orientation, mean mineralization, and mechanical properties) remain constant with age.

These differences in bone quality at the mid-diaphysis of the femur during pediatric growth translate into differences in mechanical properties. Here, strength and stiffness increased with age (**Fig. S8**), such that the mechanical resistance of the fetal/infantile bone tissue was found to be significantly lower than the 2-14 year-old cases (**Fig. 5E,F**). Therefore, the fetal/infantile tissue is

inherently weaker than the 2-14 year-old cases. In terms of a mechanistic explanation for the differences in mechanical resistance, we used synchrotron SAXS/WAXD measurements to investigate deformation in the collagen fibril and mineral, which are responsible for generating bone strength and stiffness. Our results show that the collagen fibrils deform similarly in all cases but that the contribution of the mineral to deformation increases with age (**Figs. 5D,H, S8**); in the 2-14 year-old cases, the mineral has a greater contribution to deformation than in fetal/infantile cases (*i.e.,* greater mineral-strain to tissue-strain ratio). Changes in bone quality due to aging or disease are known to directly affect bone's mechanical resistance and ultimately fracture risk.[6–9]

Here, we observed differences in bone volume fraction, collagen fiber orientation, and mineralization distribution between the fetal/infantile and 2-14 year-old cases. Mechanistically, the fetal/infantile bone tissue is inherently weaker because it consists of woven bone tissue (rather than osteonal lamellar bone, **Fig. 1**), which has overall a lower mean mineralization (**Figs. 2F, 3E**) and less longitudinally oriented collagen fibers (**Fig. 1K**).

Lower mean mineralization in the fetal/infantile cases translates into a lower modulus tissue (**Fig. 5E**). Previous studies on pathologic or callus tissue, which consists of woven bone, have shown a correspondingly lower modulus and hardness than healthy lamellar tissue.[8,44,53] Stiffness and strength result from the bone's inherent resistance to stretching and sliding of molecular level bonds. The 'brittle, reinforcing' mineral phase has a higher stiffness and strength than the organic phase. Therefore, in bone, the stiffness and strength increase as the density of mineral gradually increases.[56]

Even though, differences in collagen deformation were not observed with SAXS, the collagen fiber organization and orientation are critical to mechanical resistance, in particular longitudinally oriented collagen is highly advantageous for resisting tensile loads.[57] Thus, even though similar deformation was observed in the collagen fibers at all ages

(**Fig. 5C**), the 2-14 year-old cases have a higher percentage of collagen fibers oriented longitudinally (**Fig. 1K**) and thus the bone in these cases is better oriented to resist tensile deformation. Furthermore, the lamellar interfaces in the osteonal micro-scale structure of bone have been shown to resist crack growth by deflecting and bridging cracks.[21,22] However, areas of disorganized woven bone in Paget's disease of bone are unable to deflect and bridge cracks.[8] Thus, the lack of lamellar surfaces in primary bone could limit the sacrificial bonding or microcracking to absorb energy during loading.[19,58]

Thus, the micron-scale bone structure of the fetal/infantile bone tissue has less mechanical

resistance than the 2-14 year-old cases because of the unorganized collagen structure present in primary bone *vs.* the highly oriented collagen fibers present in the remodeled osteons. Our mechanical data suggest a transition in the mechanical behavior with age (**Fig. S8**). The transition of the mechanical behavior seems to be mainly driven by mineral distribution (**Figs. S6E, S7D, S8**) and the collagen orientation (**Fig. S5G**). OV/BV and Ot.Lc.Ar (**Fig. S5B,E**) do reflect the metabolic reorganization of the tissue with respect to aging and loading.

Our analysis used high-resolution materials-science-based methods to quantify changes in the structure and mechanical properties of a rare pediatric cohort. However, the study design is a cross-sectional comparison of different individuals. Therefore, unknown inter-individual differences (*e.g.,* genetic, variable growth/maturation, pre-/post-pubertal growth stage, or environmental factors) may be affecting some of the observed differences. Second, the exact timing of endochondral ossification, modeling, and remodeling events as well as the specific timing of the transition to superior bone quality cannot be accurately assessed here due to the limited sample size and inter-individual variability in young cohorts. Future work would try to represent all phases of growth at the mid-diaphysis as well as at the metaphyseal/epiphyseal ends

near the growth plate with both sexes to understand age- and maturity-related variability.

In light of these limitations, our results show that the age of 1 to 2 years is a critical time for building strength and stiffness in the femoral mid-diaphysis. This change in bone structure and bone quality between 1 to 2 years of age coincides with walking in humans, which creates new mechanical demands on the femoral diaphysis of infants. Indeed, in addition to the effects of genetic and hormonal factors on skeletal development, mechanobiological signals and muscular forces play a critical role in determining bone size and shape.[47,59]

Fracture incidence is high in children/adolescents and in the elderly. While fracture risk in the elderly occurs due to imbalances in bone remodeling, a different mechanism may be at play in children. In particular, the pubertal growth spurt in humans coincides with a decrease in areal bone mineral density (aBMD) and peak fracture incidence, with the most common fracture site being the distal forearm; thus, it has been suggested that the growth spurt may result in a transitory weakness in the skeleton.[11,13,16,17,60] Our results suggest that bone formed through endochondral ossification is mechanically weaker than remodeled bone due to its woven bone structure and lower mean mineralization. In particular the high incidence of distal forearm fractures in children/adolescents could relate to the formation of low quality bone (*i.e.,* woven microstructure, low bone volume fraction, low mean mineralization) adjacent to the growth plate creating a mechanically weak zone. However, further work here is needed to confirm that primary bone at the distal forearm persists in children and/or adolescents, especially during peak growth periods and results in increased fracture incidence.

In summary, during skeletal growth, ossification, modeling, and remodeling processes are actively elongating and shaping the bones that will eventually compose the mature skeleton. Here,

at the femoral mid-diaphysis, we observed differences in bone quality; in fetal/infantile cases, the bone tissue consists of a scaffold-like structure of woven bone with high osteocyte lacunar density and size produced by endochondral ossification, while in the 2-14 year old cases, remodeling of the bone structure results in a highly organized lamellar structure with a greater mean mineralization and bone volume fraction. We find that these dramatic changes in bone quality around 1-2 years of age leads to greater mechanical resistance, as collagen fibrils are better aligned to resist tensile forces and more mineral is present to reinforce the collagen scaffold. Thus, these results highlight the inherent low bone quality and mechanical weakness of the fetal/infantile

skeleton. Furthermore, endochondral ossification may produce a similarly weak, low quality bone structure at skeletal sites near growth plates (*i.e.,* proximal/distal ends of long bones).

Acknowledgments: This project was supported by the Alexander von Humboldt Foundation and the German Research Foundation (DFG) - under grant no. BU 2562/3-1/5-1. We acknowledge travel grants provided by the International Affairs, Strategy and Partnership office of the University of Hamburg. We acknowledge use of the x-ray synchrotron beamline 7.3.3 at the Advanced Light Source at Lawrence Berkeley National Laboratory, which is funded by the Office of Science of the U.S. Department of Energy under contract no. DE-AC02-05CH11231. We also acknowledge use of the beamline ID 10 at the European Synchrotron Radiation Facility. We thank Jerome Kieffer from the ESRF data analysis unit for acceleration of the phase retrieval program.

Felix Schmidt acknowledges the Joachim Herz Foundation for a PhD scholarship in cooperation with the PIER Helmholtz Graduate School, University of Hamburg and DESY Hamburg.

Authors' roles: EAZ and BB designed the experiment. EAZ, CR, FNS, KES, YC, ES, BG, FZ, MA, ROR and BB performed experiments, analyzed data, and interpreted the results. KP

performed autopsies. YC, ES, EV, FZ, MA, and ROR contributed experimental tools, technical support and conceptual advice. EAZ and BB wrote the manuscript. All authors revised the paper critically and approved the final version. EAZ takes responsibility for the integrity of the data analysis.

References

1. Burr DB. Bone quality: Understanding what matters. J Musculoskelet Neuronal Interact. 2004;4(2):184–6.

2. Zimmermann EA, Busse B, Ritchie RO. The fracture mechanics of human bone: Influence of disease and treatment. Bonekey Rep. 2015;4:743.

3. Zebaze RMD, Ghasem-Zadeh A, Bohte A, Iuliano-Burns S, Mirams M, Price RI, Mackie EJ, Seeman E.
Intracortical remodelling and porosity in the distal radius and post-mortem femurs of women: a cross-sectional study. Lancet. 2010;375(9727):1729–36.

4. Karasik D, Rivadeneira F, Johnson ML. The genetics of bone mass and susceptibility to bone diseases. Nat Rev Rheumatol. 2016;12:323–34.

5. Dempster DW, Compston JE, Meunier PJ. Bone histomorphometry and bone quality. Osteoporos Int. 2009;20(3):243–4.

6. Busse B, Bale HA, Zimmermann EA, Panganiban B, Barth HD, Carriero A, Vettorazzi E, Zustin J, Hahn M, Ager JW, Püschel K, Amling M, Ritchie RO. Vitamin D deficiency induces early signs of aging in human bone, increasing the risk of fracture. Sci Transl Med. 2013;5(193):193ra88.

7. Zimmermann EA, Schaible E, Bale H, Barth HD, Tang SY, Reichert P, Busse B, Alliston T, Ager JW, Ritchie RO. Age-related changes in the plasticity and toughness of human cortical bone at multiple length scales. Proc Natl Acad Sci USA. 2011;108(35):14416–21.

8. Zimmermann EA, Köhne T, Bale HA, Panganiban B, Gludovatz B, Zustin J, Hahn M, Amling M, Ritchie RO, Busse B. Modifications to nano- and microstructural quality and the effects on mechanical integrity in Paget's disease of bone. J Bone Miner Res. 2015;30(2):264–73.

9. Carriero A, Zimmermann EA, Paluszny A, Tang SY, Bale H, Busse B, Alliston T, Kazakia G, Ritchie RO, Shefelbine SJ. How tough is brittle bone? Investigating osteogenesis imperfecta in mouse bone. J Bone Miner Res. 2014;29(6):1392–401.

10. Donaldson LJ, Reckless IP, Scholes S, Mindell JS, Shelton NJ. The epidemiology of fractures in England. J Epidemiol Community Health. 2008;62(2):174–80.

11. Cooper C, Dennison EM, Leufkens HG, Bishop N, van Staa TP. Epidemiology of childhood fractures in Britain: A study using the general practice research database. J Bone Miner Res. 2004;19(12):1976–81.

12. Landin L, B. E. Nilsson. Bone mineral content in children with fractures. Clin Orthop Rel Res. 1983;178:292–6.

13. Hedström EM, Svensson O, Bergström U, Michno P. Epidemiology of fractures in children and adolescents. Acta Orthop. 2010;81(1):148–53.

14. C. J. Tiderius, L. Landin, H. Diippe. Decreasing incidence of fractures in children: An

epidemiological analysis
of 1,673 fractures in Malmö, Sweden, 1993–1994. Acta Orthop Scand. 1999;70(6):622–6.

15. Goulding A, Cannan R, Williams SM, Gold EJ, Taylor RW, Lewis-Barned NJ. Bone mineral density in girls
with forearm fractures. J Bone Miner Res. 1998;13(1):143–8.

16. Faulkner RA, Davison KS, Bailey DA, Mirwald RL, Baxter-Jones AD. Size-corrected BMD decreases during
peak linear growth: Implications for fracture incidence during adolescence. J Bone Miner Res.
2006;21(12):1864–70.

17. Bailey DA, Wedge JH, McCulloch RG, Martin AD, Bernhardson SC. Epidemiology of fractures of the distal
end of the radius in children as associated with growth. J Bone Joint Surg Am. 1989;71(8):1225–31.

18. Poundarik AA, Diab T, Sroga GE, Ural A, Boskey AL, Gundberg CM, Vashishth D. Dilatational band
formation in bone. Proc Natl Acad Sci USA. 2012;109(47):19178–83.

19. Fantner GE, Hassenkam T, Kindt JH, Weaver JC, Birkedal H, Pechenik L, Cutroni JA, Cidade GAG, Stucky GD, Morse DE, Hansma PK. Sacrificial bonds and hidden length dissipate energy as mineralized fibrils separate during bone fracture. Nat Mater. 2005;4(8):612–6.

20. Gupta HS, Wagermaier W, Zickler GA, Raz-Ben Aroush D, Funari SS, Roschger P, Wagner HD, Fratzl P. Nanoscale deformation mechanisms in bone. Nano Lett. 2005;5(10):2108–11.

21. Koester KJ, Ager JW, Ritchie RO. The true toughness of human cortical bone measured with realistically short cracks. Nat Mater. 2008;7(8):672–7.

22. Nalla RK, Kinney JH, Ritchie RO. Mechanistic fracture criteria for the failure of human cortical bone. Nat Mater. 2003;2(3):164–8.

23. Scherft JP. Beginning endochondral ossification in embryonic mouse radii. J Ultrastruct Res. 1973;42(3):342–53.

24. Salle BL, Rauch F, Travers R, Bouvier R, Glorieux FH. Human fetal bone development: histomorphometric evaluation of the proximal femoral metaphysis. Bone. 2002;30(6):823–8.

25. Buckwalter JA, Glimcher MJ, Cooper RR, Recker R. Bone Biology. J Bone Joint Surg Am. 1995;77(8):1276–89.

26. Rauch F. The dynamics of bone structure development during pubertal growth. J Musculoskelet Neuronal Interact. 2012;12(1):1–6.

27. Seeman E. Periosteal bone formation — A neglected determinant of bone strength. N Engl J Med. 2003;349(4):320–3.

28. Rauch F, Neu C, Manz F, Schoenau E. The development of metaphyseal cortex. Implications for distal radius fractures during growth. J Bone Miner Res. 2001;16:1547–55.

29. Seeman E, Ghasem-Zadeh A. Challenges in the acquisition and analysis of bone microstructure during growth. J Bone Miner Res. 2016;31(12):2239–41.

30. Püschel K. Lehre und Forschung an Verstorbenen. Rechtsmedizin. 2016 Apr 1;26(2):115–9.

31. Dempster DW, Compston JE, Drezner MK, Glorieux FH, Kanis JA, Malluche H, Meunier PJ, Ott SM, Recker RR, Parfitt AM. Standardized nomenclature, symbols, and units for bone histomorphometry: A 2012 update of the report of the ASBMR Histomorphometry Nomenclature Committee. J Bone Miner Res. 2013;28(1):2–

17.

32. Kulak CAM, Dempster DW. Bone histomorphometry: a concise review for endocrinologists and clinicians. Arq Bras Endocrinol Metab. 2010;54(2):87–98.

33. Goldman HM, Bromage TG, Thomas CDL, Clement JG. Preferred collagen fiber orientation in the human mid-shaft femur. Anat Rec A. 2003;272(1):434–45.

34. Boyde A, Riggs CM. The quantitative study of the orientation of collagen in compact bone slices. Bone. 1990;11(1):35–9.

35. Skedros JG, Mason MW, Nelson MC, Bloebaum RD. Evidence of structural and material adaptation to specific strain features in cortical bone. Anat Rec. 1996;246(1):47–63.

36. Bromage TG, Goldman HM, McFarlin SC, Warshaw J, Boyde A, Riggs CM. Circularly polarized light standards for investigations of collagen fiber orientation in bone. Anat Rec B. 2003;274(1):157–68.

37. Koehne T, Vettorazzi E, Küsters N, Lüneburg R, Kahl-Nieke B, Püschel K, Amling M, Busse B. Trends in trabecular architecture and bone mineral density distribution in 152 individuals aged 30–90 years. Bone. 2014;66:31–8.

38. Boskey A, Pleshko Camacho N. FT-IR imaging of native and tissue-engineered bone and cartilage. Biomaterials. 2007;28(15):2465–78.

39. Farlay D, Panczer G, Rey C, Delmas PD, Boivin G. Mineral maturity and crystallinity index are distinct characteristics of bone mineral. J Bone Miner Metab. 2010;28(4):433–45.

40. Hexemer A, Bras W, Glossinger J, Schaible E, Gann E, Kirian R, MacDowell A, Church M, Rude B, Padmore H. A SAXS/WAXS/GISAXS beamline with multilayer monochromator. J Phys: Conf Ser. 2010;247(1):12007.

41. Zimmermann EA, Gludovatz B, Schaible E, Dave NKN, Yang W, Meyers MA, Ritchie RO. Mechanical adaptability of the Bouligand-type structure in natural dermal armour. Nat Commun. 2013;4:2634.

42. Ilavsky J. Nika: software for two-dimensional data reduction. J Appl Cryst. 2012;45(2):324–8.

43. Chushkin Y, Zontone F, Lima E, De Caro L, Guardia P, Manna L, Giannini C. Three-dimensional coherent diffractive imaging on non-periodic specimens at the ESRF beamline ID10. J Synchrotron Radiat. 2014;21(3):594–9.

44. Hoerth RM, Seidt BM, Shah M, Schwarz C, Willie BM, Duda GN, Fratzl P, Wagermaier W. Mechanical and structural properties of bone in non-critical and critical healing in rat. Acta Biomater. 2014;10:4009–19.

45. Holguin N, Brodt MD, Sanchez ME, Silva MJ. Aging diminishes lamellar and woven bone formation induced by tibial compression in adult C57Bl/6. Bone. 2014;65:83–91.

46. Bortel EL, Duda GN, Mundlos S, Willie BM, Fratzl P, Zaslansky P. Long bone maturation is driven by pore closing: A quantitative tomography investigation of structural formation in young C57BL/6 mice. Acta Biomater. 2015;22:92–102.

47. Sharir A, Stern T, Rot C, Shahar R, Zelzer E. Muscle force regulates bone shaping for optimal load-bearing capacity during embryogenesis. Development. 2011;138(15):3247–59.

48. Portigliatti Barbos M, Bianco P, Ascenzi A, Boyde A. Collagen orientation in compact bone: II. Distribution of lamellae in the whole of the human femoral shaft with reference to its mechanical

properties. Metab Bone Dis
Res Res. 1984;5(6):309–15.

49. Fratzl-Zelman N, Roschger P, Misof BM, Pfeffer S, Glorieux FH, Klaushofer K, Rauch F. Normative data on
mineralization density distribution in iliac bone biopsies of children, adolescents and young adults. Bone.
2009;44(6):1043–8.

50. Currey JD, Brear K, Zioupos P. The effects of ageing and changes in mineral content in degrading the
toughness of human femora. J Biomech. 1996;29(2):257–60.

51. Currey JD, Butler G. The mechanical properties of bone tissue in children. J Bone Joint Surg. 1975;57(6):810–
4.

52. Skedros JG, Bloebaum RD, Bachus KN, Boyce TM, Constantz B. Influence of mineral content and
composition on graylevels in backscattered electron images of bone. J. Biomed. Mater. Res. 1993;27(1):57–
64.

53. Manjubala I, Liu Y, Epari DR, Roschger P, Schell H, Fratzl P, Duda GN. Spatial and temporal variations of mechanical properties and mineral content of the external callus during bone healing. Bone. 2009;45:185–92.

54. Boskey AL, Coleman R. Aging and Bone. J Dent Res. 2010;89(12):1333–48.

55. Lynch ME, Main RP, Xu Q, Schmicker TL, Schaffler MB, Wright TM, van der Meulen MCH. Tibial compression is anabolic in the adult mouse skeleton despite reduced responsiveness with aging. Bone. 2011;49(3):439–46.

56. Landis WJ, Librizzi JJ, Dunn MG, Silver FH. A study of the relationship between mineral content and mechanical properties of turkey gastrocnemius tendon. J Bone Miner Res. 1995;10(6):859–67.

57. Wagermaier W, Gupta HS, Gourrier A, Burghammer M, Roschger P, Fratzl P. Spiral twisting of fiber orientation inside bone lamellae. Biointerphases. 2006;1(1):1.

58. Zimmermann EA, Ritchie RO. Bone as a structural material. Adv Healthcare Mater. 2015;4(9):1287–304.

59. Nowlan NC, Bourdon C, Dumas G, Tajbakhsh S, Prendergast PJ, Murphy P. Developing bones are differentially affected by compromised skeletal muscle formation. Bone. 2010;46(5):1275–85.

60. Landin LA. Fracture patterns in children. Analysis of 8,682 fractures with special reference to incidence, etiology and secular changes in a Swedish urban population 1950-1979. Acta Orthop Scand Suppl. 1983;202:1–109.

Figure legends

Fig. 1. *Bone volume and collagen fiber organization during skeletal growth.* Von Kossa/van Gieson-stained sections (mineralized bone: black, unmineralized osteoid: pink) show a porous scaffold-like cortex in **(A)** fetal and **(B)** infantile cases and a dense cortex in cases between **(C)** 2 and **(D)** 14 years. **(E)** Thus, fetal/infantile cases have a 22% lower BV/TV than the 2-14 year-old cases. Rapid bone formation in fetal/infantile cases is demonstrated by the greater **(F)** OV/TV and **(G)** OS/BS compared to 2-14 year-old cases. **(H)** However, osteoid thickness was not significantly different. **(I)** Osteocyte lacunar density is substantially higher in fetal-1 year-

old cases and the **(J)** osteocyte lacunae are enlarged in fetal-1 year-old cases in comparison to 2-14 year-old cases. **(K-O)** Quantitative polarized light microscopy (bright: transverse fiber orientation, dark: longitudinal fiber orientation) measures collagen fiber orientation. **(K)** Here, the average brightness is significantly lower in the 2-14 year-old cases than the fetal/infantile cases implying that more fibers are longitudinally oriented in the older cases. Images show subsets of measured regions of interest. Histograms and bar graphs reflect characterizations of complete regions of interest. Data presented as mean ± SD. Mann-Whitney U test: * $p<0.05$. Scale bars are 500 microns. Data presented as a function of age in Fig. S5.

Fig. 2. *Bone mineralization during skeletal growth.* Quantitative backscattered electron imaging (qBEI) was used to measure the mineral density distribution (high mineralization: brighter, low mineralization: darker). In the **(A)** fetal and **(B)** infantile cases, calcified cartilage (white arrows)

and areas with new bone formation (*i.e.,* low mineralization) were observed, while the **(C)** 2 through **(D)** 14 year-old cases exhibited secondary osteons (black asterisks). **(E)** Evaluation of the gray value histograms shows the trends in **(F)** Ca Mean, **(G)** Ca Peak, **(H)** Ca Width (signifying variance/heterogeneity), **(I)** Ca High and **(J)** Ca Low. The scale bar equals 250 microns. Images show subsets of measured regions of interest. Histograms and bar graphs reflect characterizations of complete regions of interest. Data presented as mean ± SD. Mann-Whitney U test: * $p<0.05$. Data presented as a function of age in Fig. S6.

Fig. 3. *Bone matrix quality during skeletal growth.* Fourier transform infrared (FTIR) spectroscopy was used to image the quality of the bone matrix. **(A-D)** Images and histograms of the mineral-to-matrix ratio (MMR) confirm the differences in mineralization between the fetal/infantile cases and the 2-14 year-old cases. **(E)** The fetal/infantile cases have a 12% lower MMR. **(F)** The carbonate-to-phosphate ratio (CPR) and **(G)** mineral maturity were not significantly different. Data presented as mean ± SD. Images show subsets of measured regions of interest. Histograms and bar graphs reflect characterizations of complete regions of interest. Mann-Whitney U test: * $p<0.05$. Data presented as a function of age in Fig. S7.

Fig. 4. *Larger density and volume of extrafibrillar mineral platelets with age.* 3D nanostructural images of 2-month and 14-year-old bone were reconstructed at a 15-nm voxel size with synchrotron coherent x-ray diffraction imaging (CDI). **(A)** In 2D slices of the 2-month-old case, the fibril structure can be seen, where **(B)** the staggered spacing of collagen and mineral produces an alternating dark and bright pattern. **(C)** In the 3D reconstruction of the 14 year-old bone, large and bright extrafibrillar mineral particles are visible. **(D)** The extrafibrillar mineral particles are found in both the 2-month-old and 14 year-old cases; however, the size and

density of extrafibrillar
mineral was more abundant in the 14 year-old case. Here, the mineral particle volume follows a
log-normal distribution, with the 14 year-old case having a 71% greater density of extrafibrillar
mineral.

Fig. 5. *Deformation mechanisms resisting fracture during skeletal growth.* Synchrotron
experiments investigated bone's nanoscale deformation. Here, tensile tests (test specimens ≥
2/individual) were performed during synchrotron small-angle x-ray scattering (SAXS) and wide-
angle x-ray diffraction (WAXD). **(A,B)** Tensile tests measuring stress (*i.e.,* applied load/sample
area) and strain (*i.e.,* percent change in length) show differences in mechanical properties between
the fetal/infantile cases and 2-14 year-old cases. Tissue stress, mineral strain and fibril strain were
binned every 0.1% tissue strain and were aggregated at the individual level. **(C)** Fibril deformation
(SAXS) shows a linear increase in fibril strain during tensile tests for all cases. **(D)** Mineral
deformation (WAXD) measurements indicate greater mineral strain in 2-14 year-old cases. The 2-
14 year-old cases exhibited **(E)** 160% higher modulus and **(F)** 83% higher strength with trends
towards lower **(G)** failure strain. **(H)** Additionally, the slope of the mineral strain *vs.* tissue strain
is 60% higher in the 2-14 year-old cases. Data presented as mean ± SD and were fit with linear or
exponential curves. Mann-Whitney U test: * $p<0.05$. Data presented as a function of age in Fig.
S8.

Figures

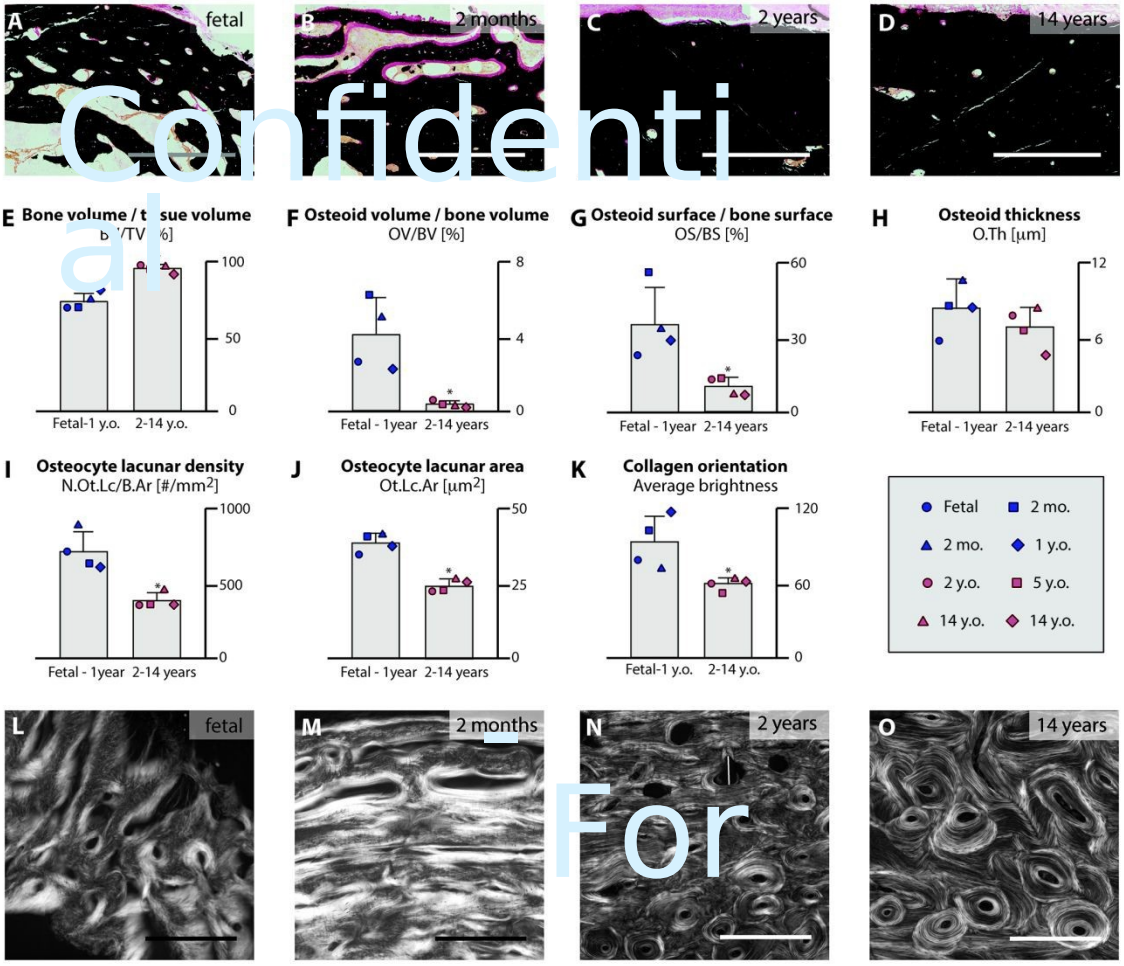

Fig. 1. *Bone volume and collagen fiber organization during skeletal growth.* Von Kossa/van Gieson-stained sections (mineralized bone: black, unmineralized osteoid: pink) show a porous scaffold-like cortex in **(A)** fetal and **(B)** infantile cases and a dense cortex in cases between **(C)** 2 and **(D)** 14 years. **(E)** Thus, fetal/infantile cases have a 22% lower BV/TV than the 2-14 year-old cases. Rapid bone formation in fetal/infantile cases is demonstrated by the greater **(F)** OV/TV and **(G)** OS/BS compared to 2-14 year-old cases. **(H)** However, osteoid thickness was not significantly different. **(I)** Osteocyte lacunar density is substantially higher in fetal-1 year-old cases and the **(J)** osteocyte lacunae are enlarged in comparison to 2-14 year-old cases. **(K-O)**

Quantitative polarized light microscopy (bright: transverse fiber orientation, dark: longitudinal fiber orientation) measures collagen fiber orientation. **(K)** Here, the average brightness is significantly lower in the 2-14 year-old cases than the fetal/infantile cases implying that more fibers are longitudinally oriented in the older cases. Images show subsets of measured regions of interest. Histograms and bar graphs reflect characterizations of complete regions of interest. Data presented as mean ± SD. Mann-Whitney U test: * $p<0.05$. Scale bars are 500 microns. Data presented as a function of age in Fig. S5.

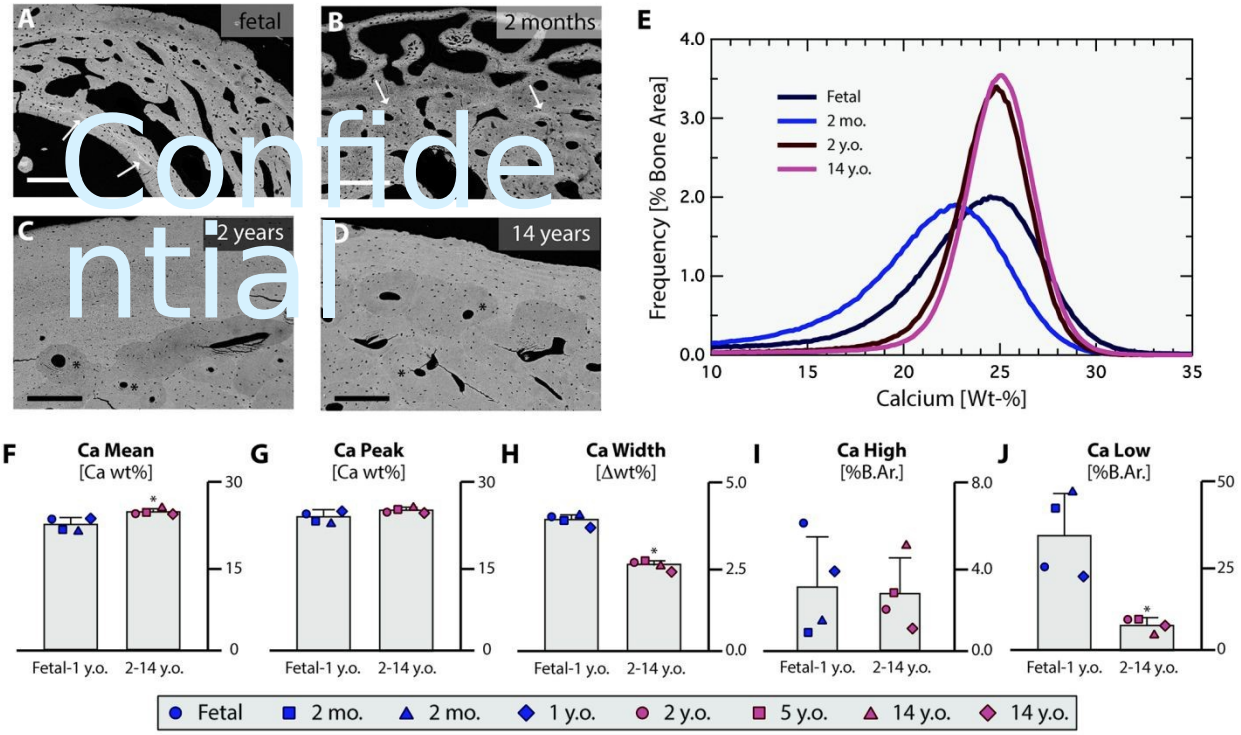

Fig. 2. *Bone mineralization during skeletal growth.* Quantitative backscattered electron imaging (qBEI) was used to measure the mineral density distribution (high mineralization: brighter, low mineralization: darker). In the **(A)** fetal and **(B)** infantile cases, calcified cartilage (white arrows) and areas with new bone formation (*i.e.,* low mineralization) were observed, while the **(C)** 2 through **(D)** 14 year-old cases exhibited secondary osteons (black asterisks). **(E)** Evaluation of the gray value histograms shows the trends in **(F)** Ca Mean, **(G)** Ca Peak, **(H)** Ca Width (signifying variance/heterogeneity), **(I)** Ca High and **(J)** Ca Low. The scale bar equals 250 microns. Images show subsets of measured regions of interest. Histograms and bar graphs reflect characterizations of complete regions of interest. Data presented as mean ± SD. Mann-Whitney U test: * $p<0.05$. Data presented as a function of age in Fig. S6.

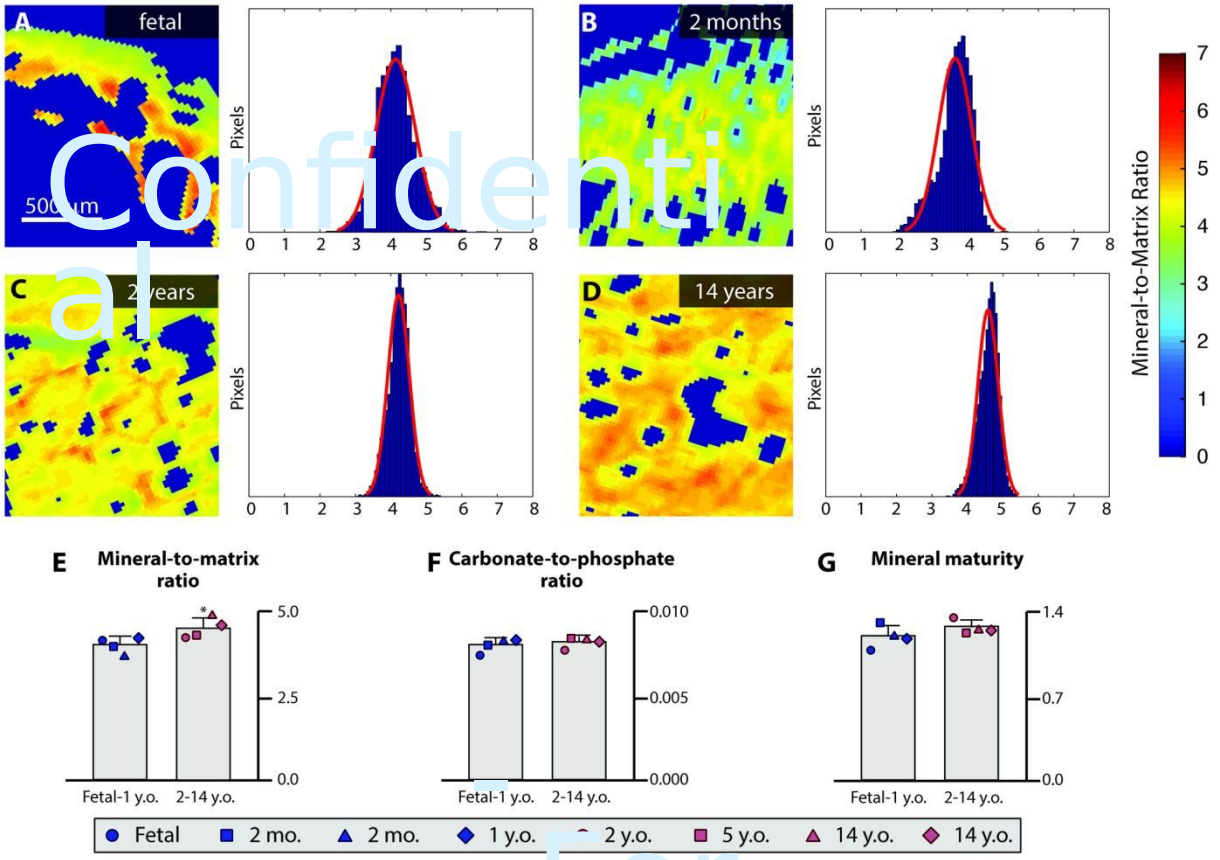

Fig. 3. *Bone matrix quality during skeletal growth.* Fourier transform infrared (FTIR) spectroscopy was used to image the quality of the bone matrix. **(A-D)** Images and histograms of the mineral-to-matrix ratio (MMR) confirm the differences in mineralization between the fetal/infantile cases and the 2-14 year-old cases. **(E)** The fetal/infantile cases have a 12% lower MMR. **(F)** The carbonate-to-phosphate ratio (CPR) and **(G)** mineral maturity were not significantly different. Data presented as mean ± SD. Images show subsets of measured regions of interest. Histograms and bar graphs reflect characterizations of complete regions of interest. Mann-Whitney U test: * $p<0.05$. Data presented as a function of age in Fig. S7.

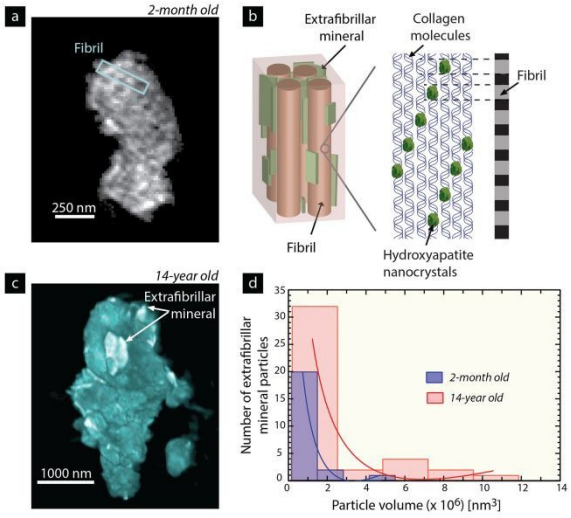

Fig. 4. *Larger density and volume of extrafibrillar mineral platelets with age.* 3D nanostructural images of 2-month and 14-year-old bone were reconstructed at a 15-nm voxel size with synchrotron coherent x-ray diffraction imaging (CDI). **(A)** In 2D slices of the 2-month-old case, the fibril structure can be seen, where **(B)** the staggered spacing of collagen and mineral produces an alternating dark and bright pattern. **(C)** In the 3D reconstruction of the 14-year-old bone, large and bright extrafibrillar mineral particles are visible. **(D)** The extrafibrillar mineral particles are found in both the 2-month-old and 14-year-old cases; however, the size and density of extrafibrillar mineral was more abundant in the 14-year-old case. Here, the mineral particle volume follows a log-normal distribution, with the 14-year-old case having a 71% greater density of extrafibrillar mineral.

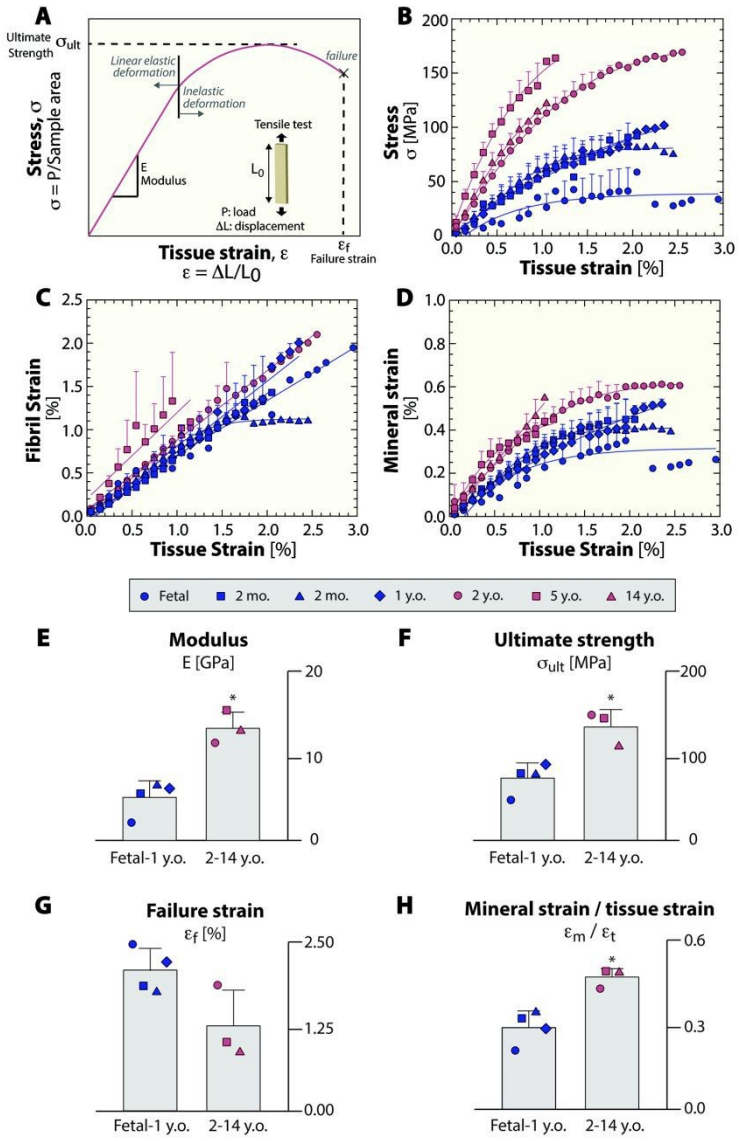

Fig. 5. *Deformation mechanisms resisting fracture during skeletal growth.* Synchrotron experiments investigated bone's nanoscale deformation. Here, tensile tests (test specimens ≥ 2/individual) were performed during synchrotron small-angle x-ray scattering (SAXS) and wide-angle x-ray diffraction (WAXD). **(A,B)** Tensile tests measuring stress (*i.e.,* applied load/sample area) and strain (*i.e.,* percent change in length) show differences in mechanical properties between the fetal/infantile cases and 2 to 14-year-old cases. Tissue stress, mineral strain and fibril strain were binned every 0.1% tissue strain and were aggregated at the individual level. **(C)** Fibril

deformation (SAXS) shows a linear increase in fibril strain during tensile tests for all cases. **(D)** Mineral deformation (WAXD) measurements indicate greater mineral strain in 2 to 14-year-old cases. The 2 to 14-year-old cases exhibited **(E)** 160% higher modulus and **(F)** 83% higher strength with trends towards lower **(G)** failure strain. **(H)** Additionally, the slope of the mineral strain *vs.* tissue strain is 60% higher in the 2-14 year-old cases. Data presented as mean ± SD and were fit with linear or exponential curves. Mann-Whitney U test: * $p<0.05$. Data presented as a function of age in Fig. S8.

Supplemental Material

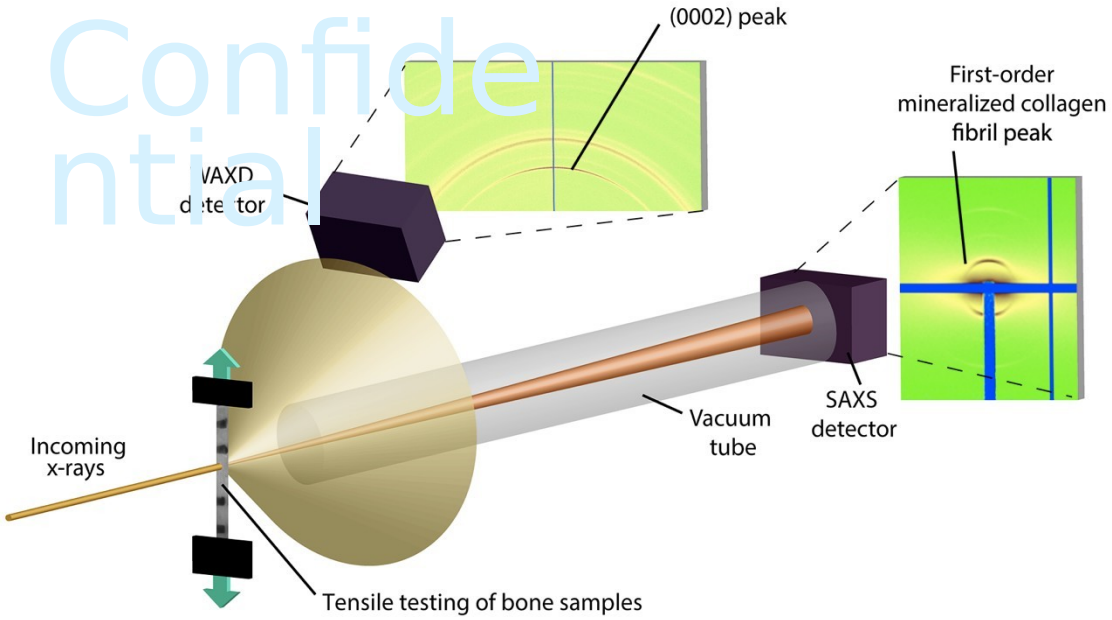

Fig. S1. *Setup of SAXS/WAXD experiments.* To measure the multi-lengthscale deformation of bone, synchrotron small-angle x-ray scattering (SAXS) and wide-angle x-ray diffraction (WAXD) experiments were performed at the Advanced Light Source synchrotron (Berkeley, CA, USA). Here, a tensile test is performed on a sample of bone tissue, while it is simultaneously exposed to a high flux x-ray source. The mineralized collagen fibrils, which are predominantly aligned with the loading direction, scatter/diffract the x-rays. Specifically, the 67-nm stagger of the mineralized collagen within the fibril diffracts the x-rays at a small angle; the position of the first-order diffraction peak can be analyzed in the tensile loading direction to measure fibril strain. Furthermore, the hexagonal structure of the hydroxyapatite mineral diffracts x-rays at wide angles. The c-axis of the mineral structure is predominantly aligned with the tensile loading direction and stretches during tensile loading, which can be measured through

changes in the position of the (0002) peak in the diffraction pattern. Through combined x-ray diffraction measurements and mechanical testing, deformation of the fibril and mineral structure can be measured at multiple time points during the mechanical test.

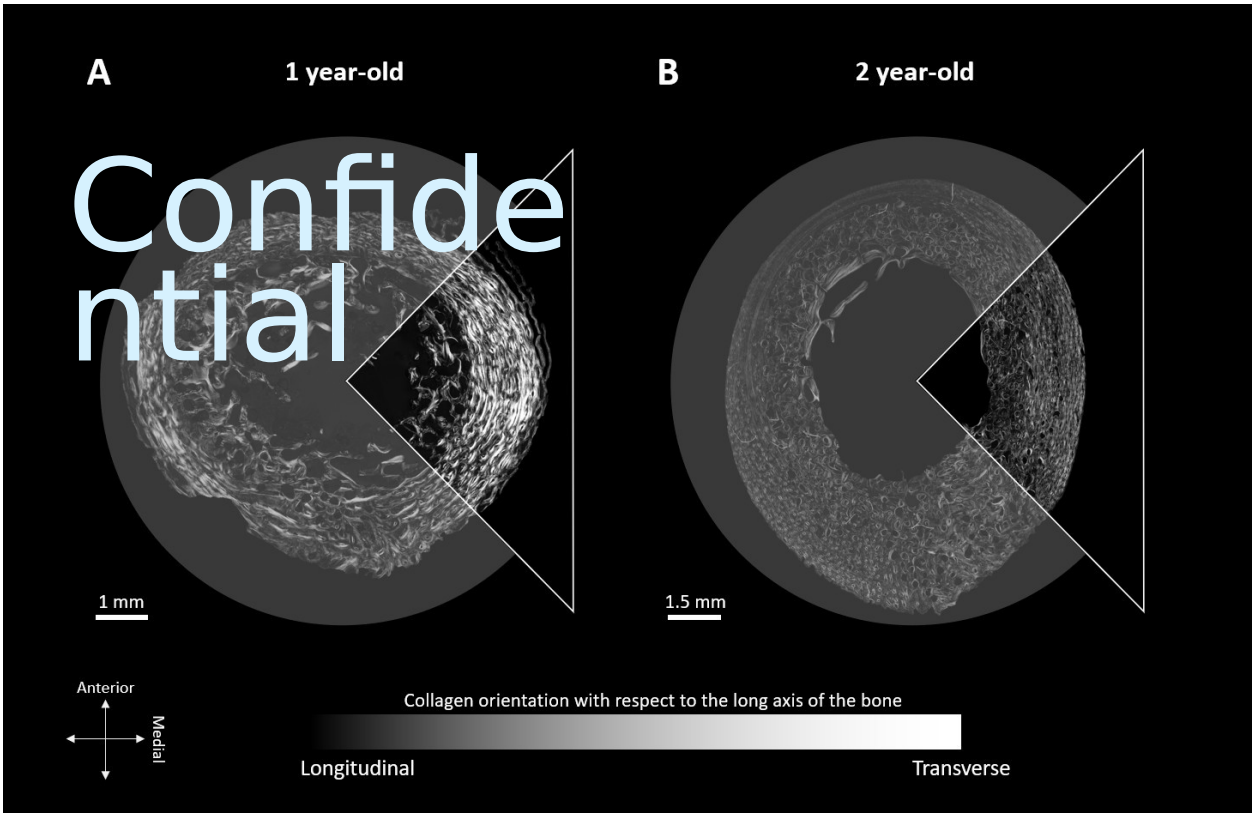

Fig. S2. *Circularly polarized light microscopy to image variations in bone structure.* A cross-section from the femoral diaphysis of the **(A)** 1 year and **(B)** 2-year-old cases imaged with circularly polarized light microscopy (CPL). In CPL, the birefringence of the collagen fibers allows the collagen fiber orientation to be imaged. Transverse fibers (with respect to the long axis of the bone) appear bright and longitudinal fibers appear dark. In addition, CPL can

discriminate changes in bone type, such as a woven vs lamellar bone structure. In the 1 year and 2 year-old cases presented here, there are clear differences in the microstructure. The 1 year-old shows predominantly woven bone, while the 2 year-old has a mix of lamellar bone and secondary osteons near the endosteal surface. Quantitative CPL data in this study were collected in the white-outlined medial axis.

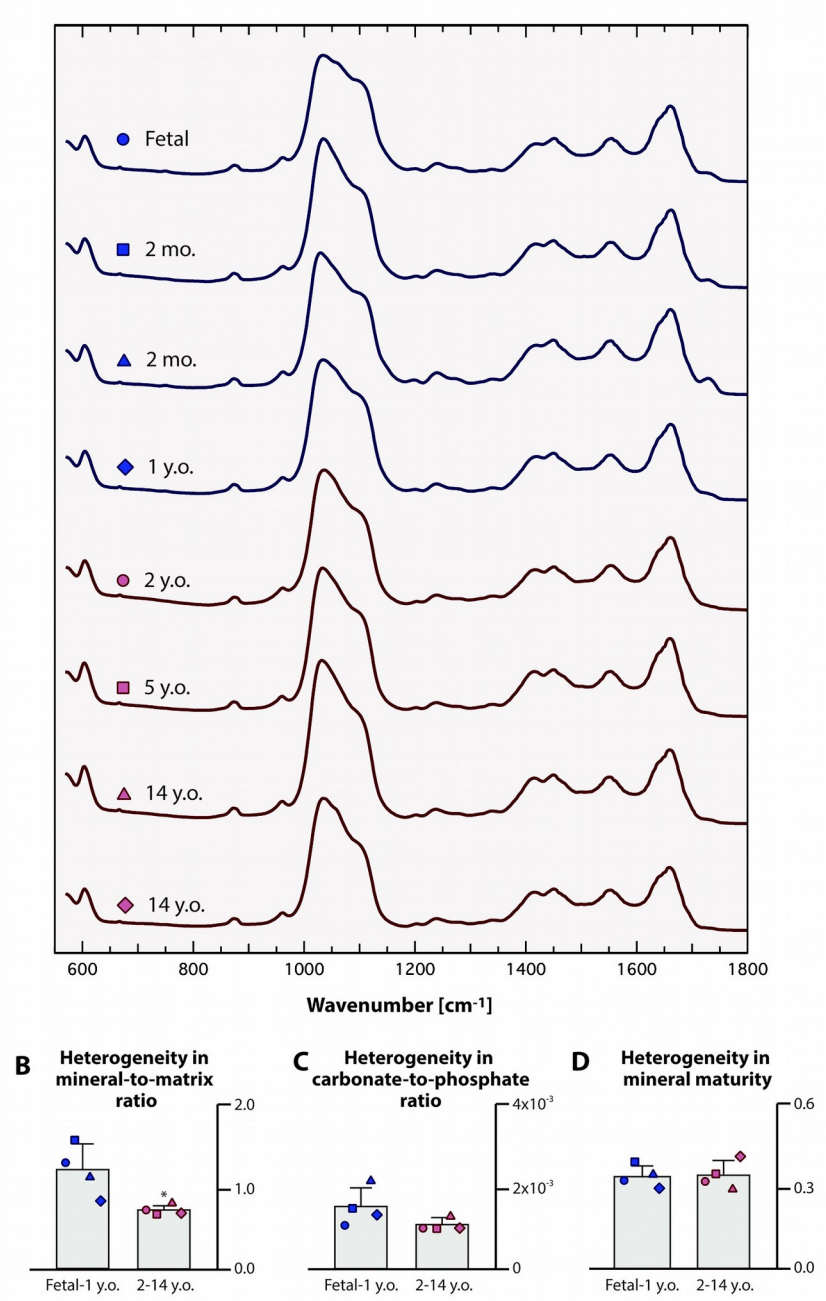

Fig. S3. *FTIR spectra and heterogeneity measurements.* Fourier transform infrared (FTIR) was used to image the quality of the bone matrix. The medial side of the cross-section of the femoral diaphysis was imaged with FTIR at a 25-μm step size. **(A)** Representative spectra from each case are shown. A number of parameters were used to assess the collagen and mineral characteristics.

The distribution of values for each individual was fit with a Gaussian curve. The full-width-at-half-max of the Gaussian curve was used to assess the heterogeneity of the distribution. The heterogeneity of the **(B)** mineral-to-matrix ratio **(C)** carbonate-to-phosphate ratio and **(D)** the mineral maturity are shown. Data are presented as mean ± SD. Mann-Whitney U test :* $p<0.05$.

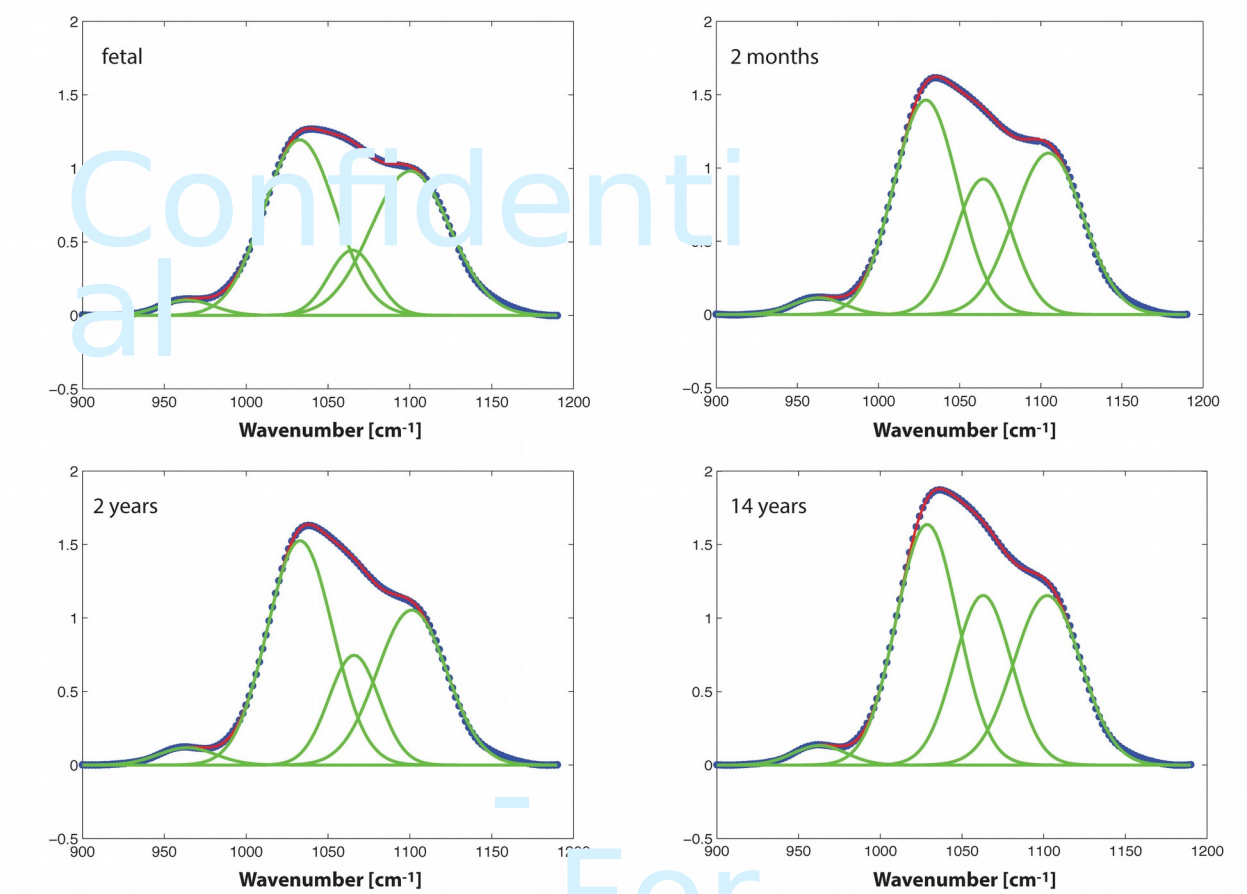

Fig. S4. *FTIR curve fitting of phosphate band for mineral maturity index.* Fourier transform infrared (FTIR) spectroscopy was used to image the quality of the bone matrix. The area ratio of the 1030 to 1110 cm^{-1} subbands provides a measure of the mineral maturity index. Here, representative spectra for the fetal, 2-month-old, 2-year-old and 14-year-old cases are shown (blue dots) along with the curve fit line (red) and the four Gaussian subbands (green).

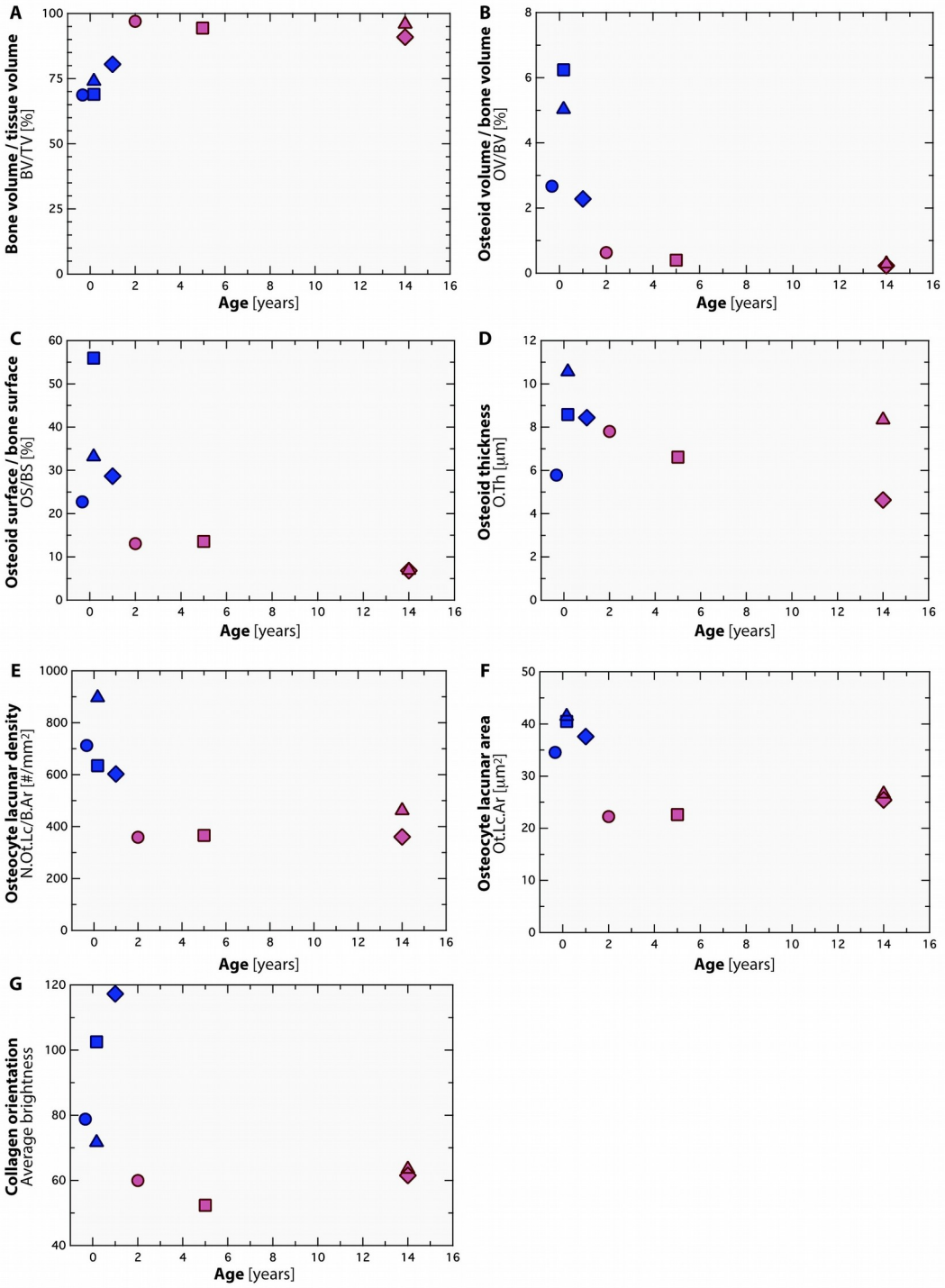

Fig. S5. *Histological and morphometric parameters as a function of age.* The histological and morphometric parameters presented in Fig. 1 are plotted here as a function of age: **(A)** bone

volume / tissue volume (BV/TV), **(B)** osteoid volume / bone volume (OV/BV), **(C)** osteoid surface / bone surface (OS/BS), **(D)** osteoid thickness (O.Th), **(E)** osteocyte lacunar density (N.Ot.Lc/B.Ar), **(F)** osteocyte lacunar area (Ot.Lc.Ar), and **(G)** collagen orientation.

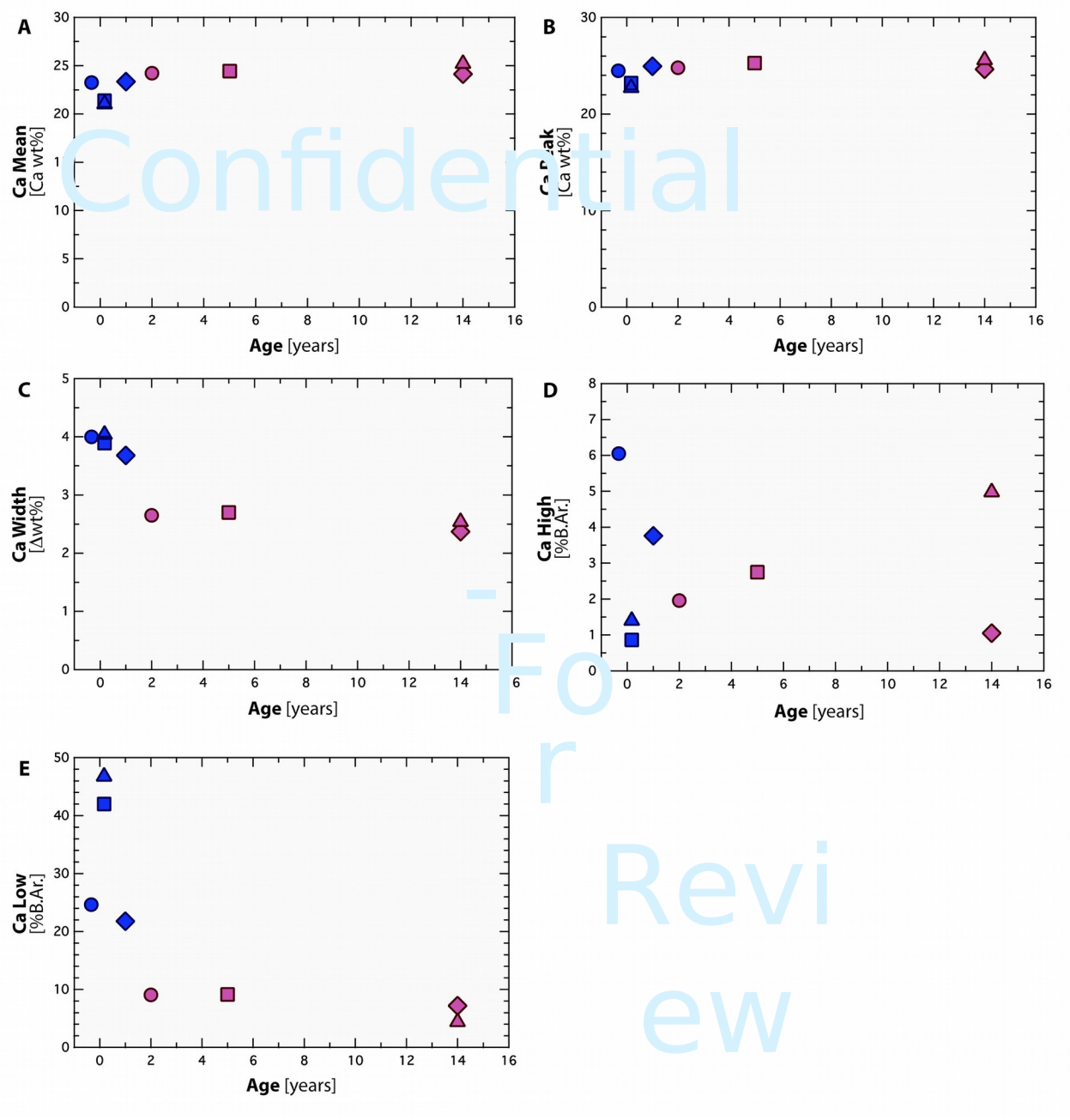

Fig. S6. *Mineralization parameters as a function of age.* Quantitative backscattered electron imaging was used to quantify the mineralization distribution. The parameters describing the bone

mineral density distribution (presented in Fig. 2) are shown here as a function of age: **(A)** Ca Mean, **(B)** Ca Peak, **(C)** Ca Width, **(D)** Ca High and **(E)** Ca Low.

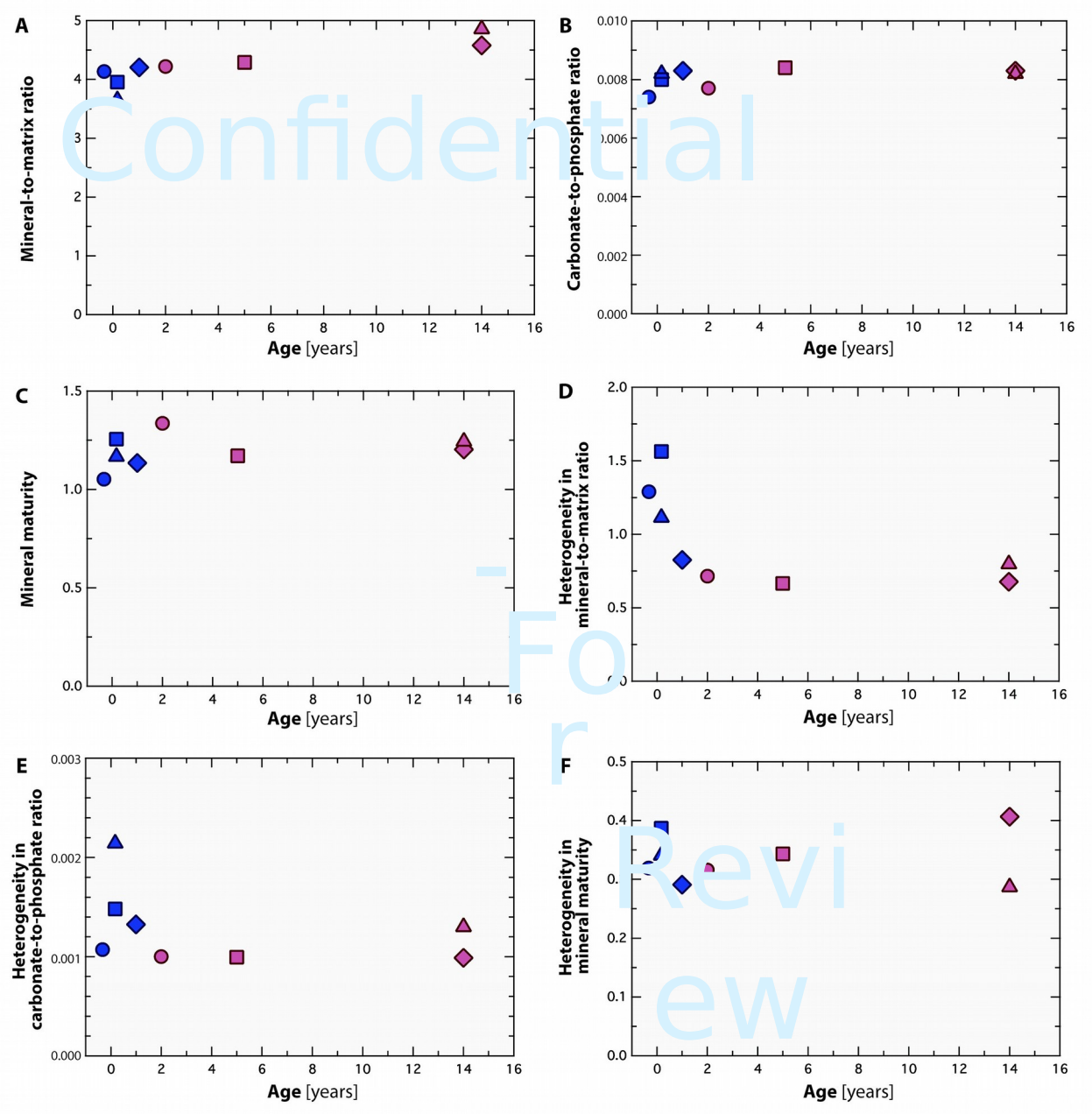

Fig. S7. *Bone matrix characteristics measured with FTIR.* Fourier transform infrared (FTIR) spectroscopy was used to image the quality of the bone matrix. The FTIR parameters presented in Fig. 3 and Fig. S3 are plotted here as a function of age: **(A)** mineral-to-matrix ratio, **(B)** carbonate-to-phosphate ratio, **(C)** mineral maturity, **(D)** heterogeneity of the mineral-to-matrix

ratio, **(E)** heterogeneity of the carbonate-to-phosphate ratio, and **(F)** heterogeneity of the mineral maturity.

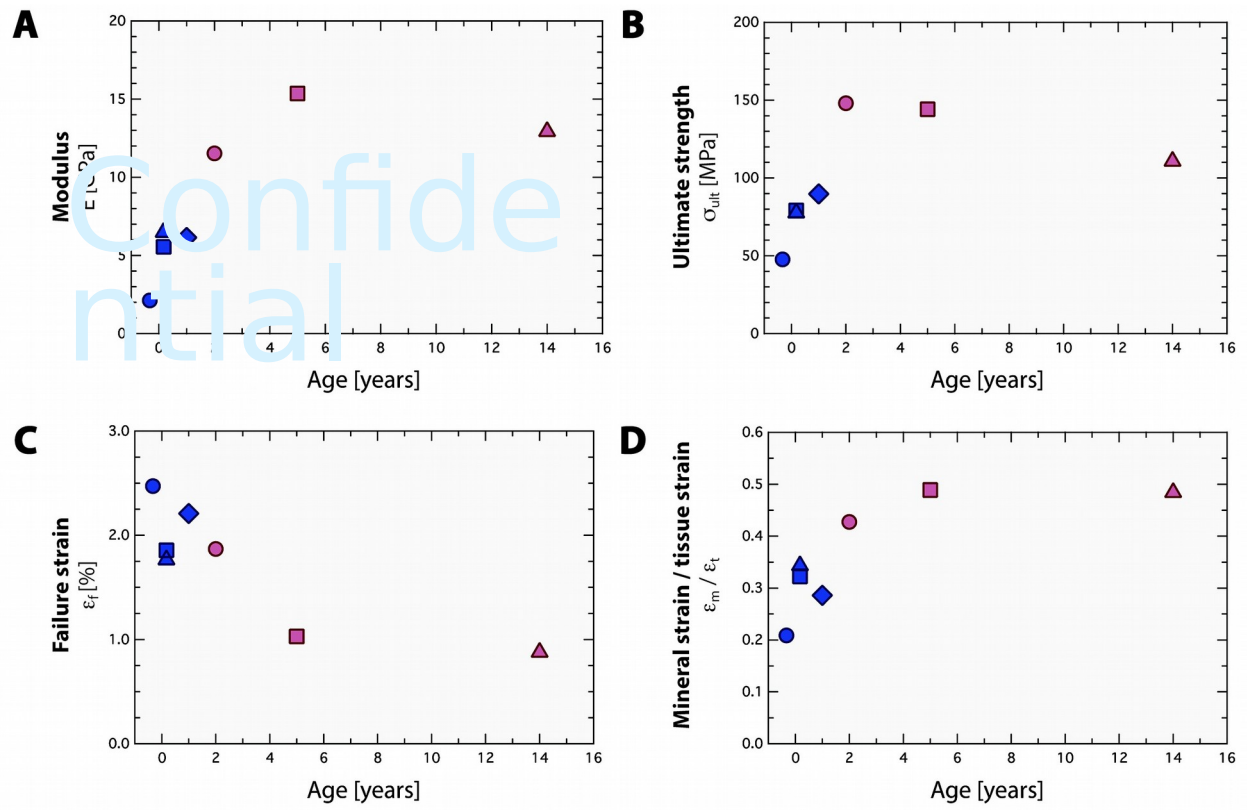

Fig. S8. *Mechanical properties as a function of age.* Tensile tests during synchrotron small- and wide-angle x-ray scattering/diffraction experiments were performed to measure deformation in the bone tissue. The mechanical properties presented in Fig. 5 are shown here as a function of age: **(A)** Young's modulus, **(B)** ultimate strength, **(C)** failure strain and **(D)** mineral strain / tissue strain.